Journal of Alloys and Compounds 648 (2015) 1031–1037

Contents lists available at ScienceDirect

Journal of Alloys and Compounds

journal homepage: http://www.elsevier.com/locate/jalcom

Influence of Zr content on the incipient melting behavior and stress-rupture life of CM247 LC nickel base superalloy

M. Mostafaei*, S.M. Abbasi

Metallic Materials Research Center, Malek Ashtar University of Technology, Tehran, Iran

ARTICLE INFO

Article history:
Received 25 April 2015
Received in revised form
22 June 2015
Accepted 13 July 2015
Available online 15 July 2015

Keywords:
CM247 LC
Incipient melting
γ/γ′ eutectic
γ′ volume fraction
Stress-rupture life

ABSTRACT

In the present work, a mechanism was proposed for secondary γ′ growth and incipient melting associated with Zr content in CM247 LC nickel base superalloy. In order to evaluate the onset temperature of incipient melt and its effect on stress-rupture life at 200 MPa/980 °C, several solution treatments were performed at 1220 °C, 1230 °C and 1250 °C on two different 0.1 and 0.4 wt% Zr content alloys. The results showed that an increase in Zr content from 0.1 to 0.4 wt% enhances the volume fraction of γ/γ′ eutectic phase from about 6% to 14% in as-cast microstructure. This phenomenon was attributed to the enhancing of γ′ former elements microsegregations in the interdendritic regions. Several heat treatments results showed that the incipient melting temperature of CM247 LC-0.4% Zr is less than 1220 °C, due to the presence of low-melting point intermetallic especially NiZr, while for CM247 LC-0.1% Zr, this temperature is over 1250 °C. Therefore the stress-rupture life for the 0.1% Zr alloy heat treated at 1230 °C is about three-fold higher than that of 0.4% Zr alloy. Also with increasing solution treatment temperature from 1220 °C to 1230 °C, the stress-rupture life of 0.1% Zr alloy has increased due to the higher volume fraction of γ′ phase. Furthermore for the 0.4% Zr alloy, with increasing solution treatment temperature from 1220 °C to 1230 °C, stress-rupture life is reduced due to the incipient melting affected by low-melting point phases such as NiZr and Ni_5Zr.

1. Introduction

CM247 LC nickel base superalloy was supplied at the request of turbine engine companies in 1978, is the latest product of first-generation directionally solidified superalloys made by Cannon Muskegon Company. This alloy is capable to pass severe temperatures and stresses conditions of blades and vanes applications [1,2]. In addition, it has the best creep properties among the first generation directionally solidified commercial superalloys and competes with the Rene N5 single crystal alloy [3]. CM247 LC is the modified version of MAR-M247 with reduced Hf, Ti and C for decreasing microsegregations, and reduced W, Co, Mo and Cr to minimize M_6C carbide and TCP phases [4–8]. TCP precipitates are rich in refractory elements such as W, Co, Cr and Mo and precipitate in the austenite matrix and greatly reduce the creep life of superalloy [9–11].

Studies have shown that increasing Zr content from 0.015 to 0.15 wt% (weight percent) in CM247 LC superalloy causes the dissolution of Zr atoms into MC carbide and morphology change from acicular or Chine's script to round shape. This morphological evolution increases the stress-rupture life from 40 to 150 h at 725 MPa/760 °C [12]. It has been reported that in superalloys such as IN100, the increase of Zr from 0.02 to 0.08 at% (atomic percent), leads to enriching MC in Zr during heat treatment and transforming to stable ZrC carbides as an in situ transformation, thereby increasing the stress-rupture life [13]. Moreover, increasing Zr content from 0.01 to 0.19 wt% stabilized the MC carbides in IN713 superalloy and inhibited its transformation into $M_{23}C_6$ at high temperatures exposure [14]. In the same research 0.1 wt% Zr was found as the optimized amount, which could result in the longest rupture time. The positive effect of Zr addition on creep properties crucially depends on the solution annealing regime. This is because excessive Zr leads to severe microsegregations and the formation of Ni_XZr_Y or ZrS phases in the interdendritic zones, both of which may increase the risk of incipient melting at high temperatures [15]. In Nimonic 80A, the increase of Zr from 0.01 to 0.05 wt% leads to a decrease in the solidus temperature from 1300 to 1170 °C due to the formation of ZrS. Such low-melting point phases may give rise to incipient melting during heat treatment and premature failing at

* Corresponding author.
E-mail address: m_mostafaei@mut.ac.ir (M. Mostafaei).

http://dx.doi.org/10.1016/j.jallcom.2015.07.104
0925-8388/

Table 1
Chemical compositions of cast alloys with two different Zr content (wt%).

Alloy	Co	W	Cr	Ta	Al	Ti	Hf	Mo	C	B	Zr[a]	S
CM247-0.1 Zr	9.65	9.42	8.01	3.51	5.54	0.80	1.05	0.45	0.08	0.01	0.11	0.006
CM247-0.4 Zr	9.61	9.04	8.50	3.40	5.53	0.78	1.02	0.41	0.08	0.01	0.41	0.005

[a] Zr content was accurately determined using ICP-AES system.

Table 2
Solution heat treatment and aging cycles for stress-rupture and incipient melting formation tests.

Test type	Cycle no.	Solution heat treatment	Aging
Stress rupture	1	1220 °C/2 h + 1230 °C/4 h + AC	1080 °C/4 h/AC + 870 °C/20 h/AC
	2	1220 °C/6 h + AC	
Incipient melting formation	3	1220 °C/2 h + AC	
	4	1230 °C/2 h + AC	
	5	1250 °C/2 h + AC	

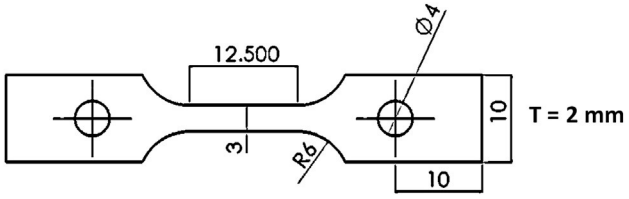

Fig. 1. Schematic of stress-rupture specimen with sub-size dimensions.

service conditions [16]. The reports on the incipient melting in DZ38 [17] and IN792 [18] support the detrimental effect of Zr-rich precipitates.

The current literature survey indicates that Zr in nickel base superalloys plays opposite roles depending on its content. The optimum amount to affect the rupture life in a positive way should be studied for each alloy individually. Hence, current investigation aimed at shedding light on the novel effect of Zr on decomposition of primary γ′ precipitates and secondary γ′ precipitates growth during heat treating and detection of Ni_5Zr or NiZr intermetallics as the main agents for incipient melting phenomenon CM247 LC superalloy.

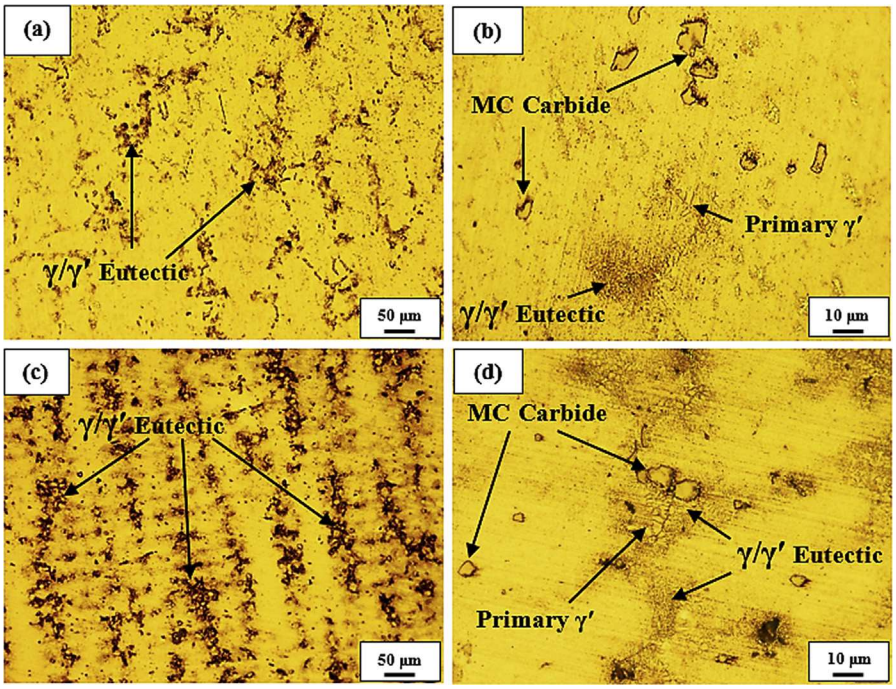

Fig. 2. Optical micrographs showing the as-cast microstructures of: a),b) CM247-0.1 Zr, c),d) CM247-0.4 Zr alloys.

Table 3
Comparison between volume fraction, SDAS, carbides volume fraction and hardness of the studied alloys.

Superalloy	Volume fraction of γ/γ′ eutectic (%)	SDAS (μm)	Volume fraction of carbide (%)	Hardness (HV)
CM247 – 0.1 Zr	6 ± 0.4	41 ± 2	2 ± 0.2	456 ± 3
CM247 – 0.4 Zr	14 ± 0.7	40 ± 1	2.4 ± 0.3	430 ± 3

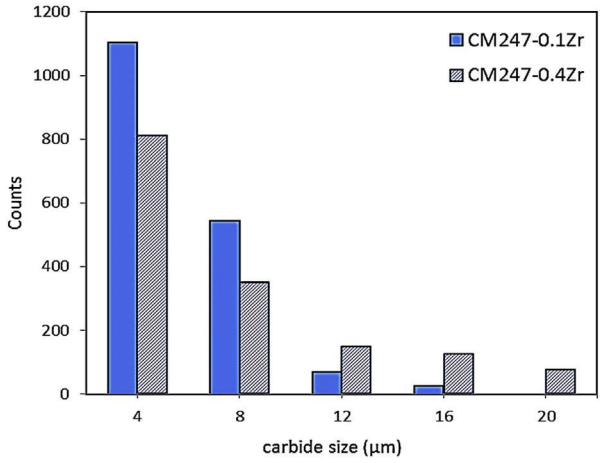

Fig. 3. Carbide size distribution in the as-cast CM247-0.1 Zr and CM247-0.4 Zr alloys.

2. Materials and methods

The alloys used in this research were melted and cast in a vacuum induction melting (VIM) furnace, with two different Zr contents of 0.1 and 0.4 wt%. The alloys were poured at about 1450 °C into an alumina mold. The ceramic mold was preheated and maintained at 1000 °C until pouring. The chemical compositions of the cast superalloys were determined using OXFORD Optical Emission Spectrometer (OES) and Zr content was accurately determined using Perkin Elmer 5300 Induction Coupled Plasma-Atomic Emission Spectrometer (ICP-AES) system. The chemical compositions of the alloys are given in Table 1.

In order to determine the γ′ solvus, incipient melting, MC carbide dissolution and liquidus temperatures of the as-cast CM247-0.1 Zr and CM247-0.4 Zr superalloys, differential scanning calorimetry (DSC) experiments were carried out in a Mettler Toledo testing apparatus (model TGA/DSC 1 Star), using a heating rate of 10 °C/min from 25 to 1400 °C. The DSC cylindrical samples with 100 mg each were cut from the cast alloys. All tests were conducted in a purged high-purity argon atmosphere using high-purity alumina crucibles. X-ray diffraction (XRD) analyses were carried out on phase extracted samples taken from the cast alloys. XRD measurements were performed in a PANalytical apparatus (model

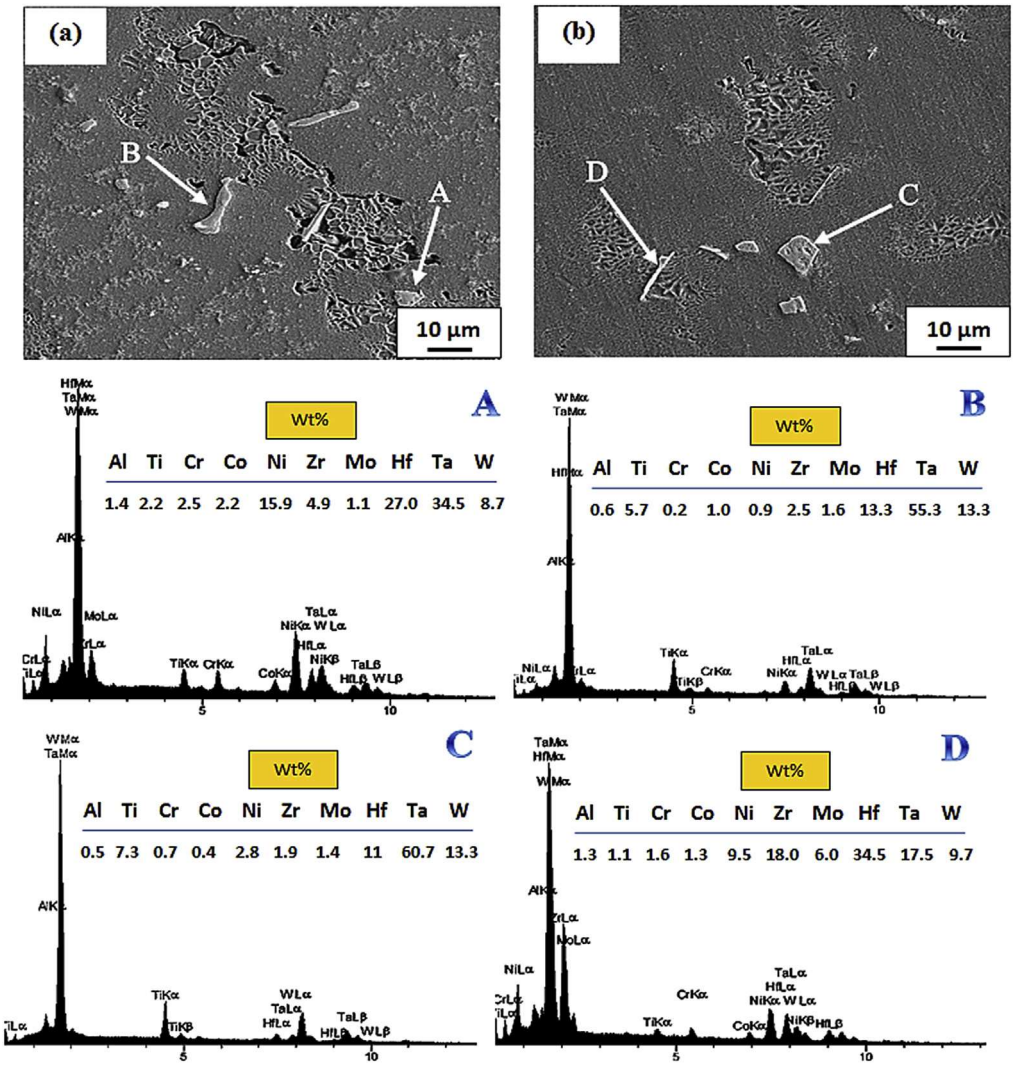

Fig. 4. SEM micrographs and EDS analyses of carbides in the as-cast microstructures: a) CM247-0.1 Zr, b) CM247-0.4 Zr.

X'Pert Pro MPD), using Cu anode at 40 kV, in a range of 10–80° with accuracy of 0.02° per each step. Stress-rupture tests performed at 200 MPa/980 °C on the solution heat treated alloys, heat treating cycles 1 and 2 according to Table 2. Also heat treating cycles 3, 4 and 5 were performed (see Table 2) in order to evaluate the microstructure and temperature associated with incipient melting. All specimens were subjected to an identical two-step aging after solution treating. Stress-rupture specimens were machined and prepared with sub-size dimensions according to Fig. 1.

For microstructural examination, the specimens were polished and etched in solutions composed of 50 mL HCl + 50 mL H_2O + 10 g $CuSO_4$ and 15 mL HCl + 10 mL HNO_3 + 10 mL Acetic acid + 2–5 drops Glycerol for detection of dendritic structure and γ′ precipitates, respectively. In addition metallographic images were observed on an Olympus BX 51optical microscope (OM) and TESCAN (model VEGA3 XMU/LaB_6 gun) scanning electron microscope (SEM) equipped with energy dispersive spectroscopy (EDS) analysis.

3. Results and discussion

The microstructures of as-cast CM247-0.1 Zr and CM247-0.4 Zr alloys are illustrated in Fig. 2. A quantitative metallography analysis using ImageJ software showed that the volume fraction of γ/γ′ eutectic in CM247-0.1 Zr is about 6%, while in CM247-0.4 Zr it is 14%. This implies that increase of Zr in the melt raises the amount of microsegregation significantly in the interdendritic regions during solidification and consequently enhances the fraction of γ/γ′ eutectic. Zhou et al. [19], through a work on M951, similarly found that the increase of Zr from 0.04 to 0.12 wt% could enhance the volume fraction of γ/γ′ eutectic up to an order of magnitude.

A comparison between secondary dendrite arm spacing (SDAS), volume fraction of γ/γ′ eutectic and hardness of both alloys is given in Table 3. The identical SDASs show that both alloys have been solidified at a similar cooling rate. However, the higher hardness of CM247 LC-0.1 Zr comparing to that of the CM247 LC-0.4 Zr could be attributed to the narrow carbide size range (between 2 and 10 μm) and uniform distribution of carbides. The carbides size and distribution for both alloys have been summarized in Fig. 3.

SEM micrographs and EDS results of carbides are shown in Fig. 4. The EDS results illustrates that in as-cast CM247-0.4 Zr alloy, MC carbides are rich in Hf, Ta and Zr, while in as-cast CM247-0.1 Zr alloy, MC carbides are rich only in Hf and Ta. Due to higher Zr content in the CM247-0.4 Zr alloy, MC carbides are observed in two morphologies marked as “C” and “D” in Fig. 4.

Therefore, it can be concluded that in CM247-0.4 Zr alloy, blocky MC carbides are usually rich in Ta and Hf, while acicular MC carbides have higher concentrations of Hf and Zr. These observations are in agreement with similar study in the literature [12].

Fig. 5 shows the SEM micrographs of the studied alloys after solution treating cycles 3, 4 and 5. The images show that incipient melting temperature of CM247-0.1 Zr is above 1250 °C; whereas for

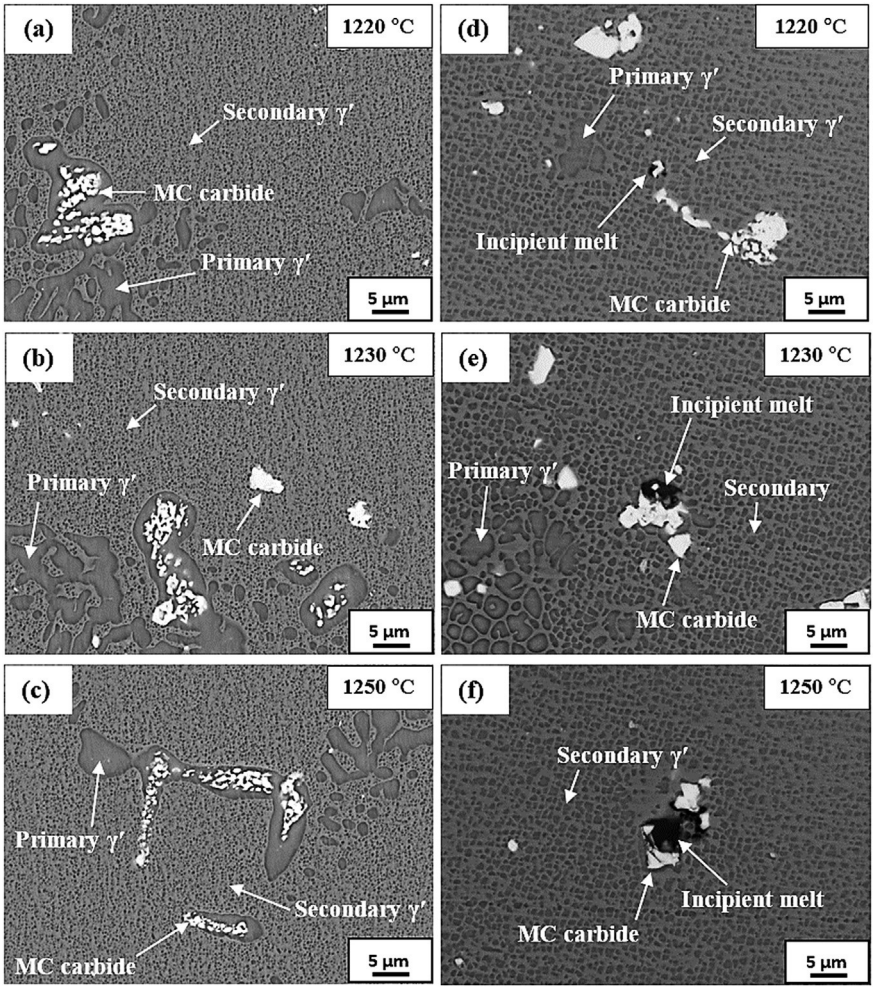

Fig. 5. SEM micrographs (BSE mode) after 2 h solution treating at 1220 °C, 1230 °C and 1250 °C + two-step aging: a),b) and c) CM247-0.1 Zr, d),e) and f) CM247-0.4 Zr superalloys.

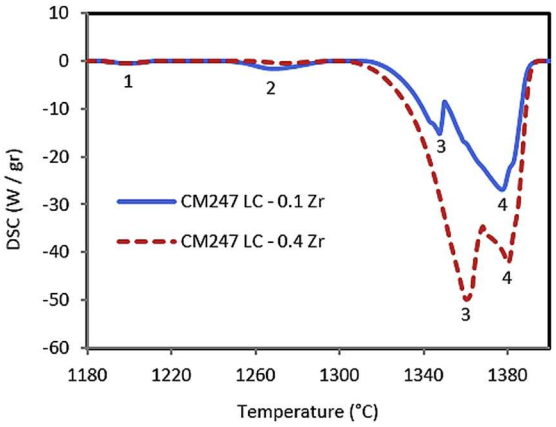

Fig. 6. DSC curves (heating cycle) for the studied superalloys.

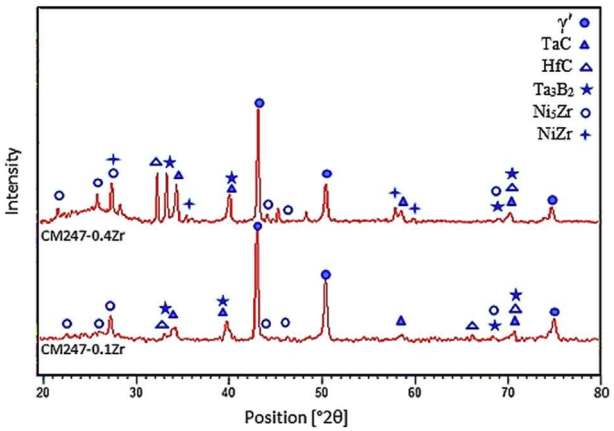

Fig. 7. XRD pattern of extracted phases from as-cast CM247-0.1 Zr and CM247-0.4 Zr superalloys.

case of CM247-0.4 Zr, the arrowed regions illustrate the onset of incipient melting at 1220 °C. It is also observed that incipient melting zones expand as temperature increases to 1230 °C and 1250 °C. Low incipient melting temperature of CM247-0.4 Zr is probably due to greater tendency for the formation of Ni_XZr_Y easy-melting intermetallics during heat treatment. Fig. 5 illustrates smaller primary γ′ precipitates in CM247-0.4 Zr alloy with a lower volume fraction compared to CM247-0.1 Zr alloy. This is fair to say that increasing Zr accelerates the decomposition of primary γ′ precipitates and going into γ solid solution during solution treatment.

Therefore, during the aging heat treatment, the secondary γ′ precipitates grow faster and would be coarser after two-step aging. As a result, after two-step aging in CM247-0.1 Zr the size of secondary γ′ precipitates is within 200–400 nm, while in CM247-0.4 Zr that falls in range of 500–900 nm.

Similar results were also reported by Xie et al. [20] for GH586 superalloy. They observed that the increase of Zr from 0.02 to 0.08 wt% would raise the size of secondary γ′ precipitates from 300 to 400 nm and its volume fraction for about 3%. They also found that this, in parallel, ameliorated the stress-rupture life of the alloy.

DSC curves (heating cycle) for the studied superalloys are depicted in Fig. 6. The types of transformations and corresponding temperatures of each peak in the DSC curves of Fig. 6 are given in Table 4. The DSC results indicate that the increase of Zr in CM247 LC superalloy increases the dissolution temperature of MC carbides. As mentioned before, the thermal stability of MC carbide increases with the dissolution of Zr atoms in their atomic lattice. This is easily elicited from the increase in the area under the DSC curve of CM247-0.4 Zr in the temperature range of 1320–1370 °C (Fig. 6), which indicates the thermal energy consumed for carbide dissolution. In another words, it is concluded that carbides with higher Zr content are more stable. From the thermodynamic point of view, the literature supports these findings. Because, the Gibbs free energy of formation for various carbides indicates that HfC is the most stable one and ZrC is more stable than TaC [21]. Thus, (Hf, Zr)C in CM247-0.4 Zr should be more stable than (Hf,Ta)C in CM247-0.1 Zr.

According to the results of DSC, the temperatures of γ′ dissolution (peak 1) and γ matrix melting transformation (peak 4) are nearly independent of Zr levels; because Zr dissolution in γ′ and γ phases is negligible. Besides, the temperature associated with peak 2 (γ/γ′ eutectic) in CM247-0.4 Zr is more than it in CM247-0.1 Zr, which indicates dependency upon γ/γ′ eutectic volume fraction.

The XRD patterns of extracted phases from the studied superalloys are shown in Fig. 7 reveals the peaks pertaining to γ′ precipitates, Ta and Hf rich MC carbides and grain boundary phases such as borides (M_3B_2 and Ta_3B_2) and Zr intermetallic compounds (Ni_5Zr and NiZr) in both alloys. The main difference between the XRD spectrums is in the peaks of Ni_XZr_Y intermetallics. As seen, in CM247-0.4 Zr alloy the peaks of Ni_5Zr and NiZr phases can be observed, while in CM247-0.1 Zr alloy only that of Ni_5Zr is discernible.

These results are consistent with the observations on the low temperature incipient melting in CM247-0.4 Zr. Previous studies have confirmed that NiZr phase forms low melting point microstructural constituent, and is probably part of multiphase eutectics which is the main agent for decreasing the incipient melting temperature in superalloys with high Zr contents [22].

The results of stress-rupture tests of CM247-0.1 Zr and CM247-0.4 Zr superalloys (at 200 MPa/980 °C) for two solution treatments (cycles 1 and 2) are shown in Fig. 8. Further details for the results of

Table 4
Results obtained from the DSC curves of Fig. 7, characterizing the transformations and corresponding temperatures.

Transformation	Peak no.	CM247 LC – 0.4 Zr	CM247 LC – 0.1 Zr
γ′ Dissolution	1	1202 °C	1201 °C
γ/γ′ Eutectic dissolution	2	1275 °C	1270 °C
MC Carbide dissolution	3	1367 °C	1354 °C
γ Matrix melting	4	1384 °C	1384 °C

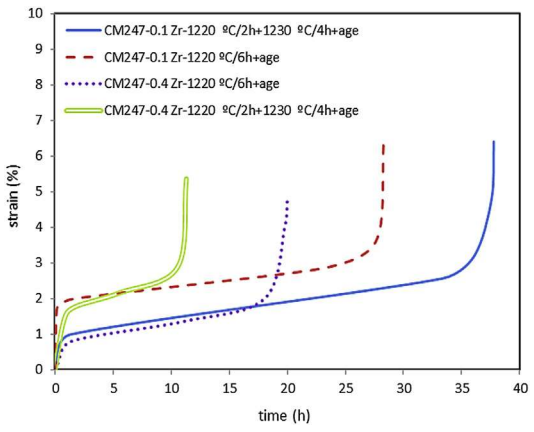

Fig. 8. Results of stress-rupture tests of CM247-0.1 Zr and CM247-0.4 Zr superalloys (at 200 MPa/980 °C) for two solution heat treatments (cycles 1 and 2) as strain versus time curves.

Table 5
Details of stress-rupture test results for CM247-0.1 Zr and CM247-0.4 Zr superalloys (at 200 MPa/980 °C).

Alloy	Heat treatment	γ′ volume fraction	Time to fracture (hr)	El%
CM247 LC – 0.1% Zr	1220 °C/6 h + age	53%	28	4%
	1220 °C/2 h + 1230 °C/4 h + age	57%	38	4%
CM247 LC – 0.4% Zr	1220 °C/6 h + age	48%	20	2%
	1220 °C/2 h + 1230 °C/4 h + age	51%	11.5	3%

stress-rupture tests are given in Table 5.

In CM247-0.1 Zr alloy, the increasing of solution treatment temperature has elevated the γ′ volume fraction from 53 to 57% and has changed the morphology of secondary γ′ to more cuboidal shape. As a result, the rupture life has increased from 28 to 38 h. However, in CM247-0.4 Zr alloy despite an increase in the γ′ volume fraction from 48 to 51% due to the increase in solution treatment temperature, the rupture life has decreased from 20 to 11.5 h. This behavior is associated with the large incipient melting zones observed in Fig. 5. Therefore as the incipient melting area grows with increasing solution annealing temperature, the rupture life tends to decrease. SEM images (Fig. 9) illustrate the size, distribution and volume fraction of the secondary γ′ phases in CM247-0.1 Zr and CM247-0.4 Zr alloys at different heat treating conditions.

As mentioned, the significant coarsening of secondary γ′ precipitates in CM247-0.4 Zr alloy during aging (Fig. 9) is known due to the contribution of Zr atoms in increasing the lattice parameter of γ′. EDS analysis indicated about 2 wt% Zr in γ′ phase as $(Ni, Co, Cr)_3(Al, Ti, Ta, Zr)$ form shown in Fig. 10 and Table 6. As a result of this, γ′ lattice coherency in the γ matrix reduces and less energy is therefore required for its coarsening [20].

In both alloys, the γ′ volume fraction has increased with an increase in the temperature of solution. Since, the higher the solution temperature is, the more solution of γ′ and γ/γ′ eutectic into γ and the higher volume fraction of secondary γ′ will be. Also as noted earlier in Fig. 5, the primary γ′ precipitates in CM247-0.4 Zr alloy are smaller and have lower volume fraction, comparing to CM247-0.1 Zr, indicating that an increase in Zr accelerates the

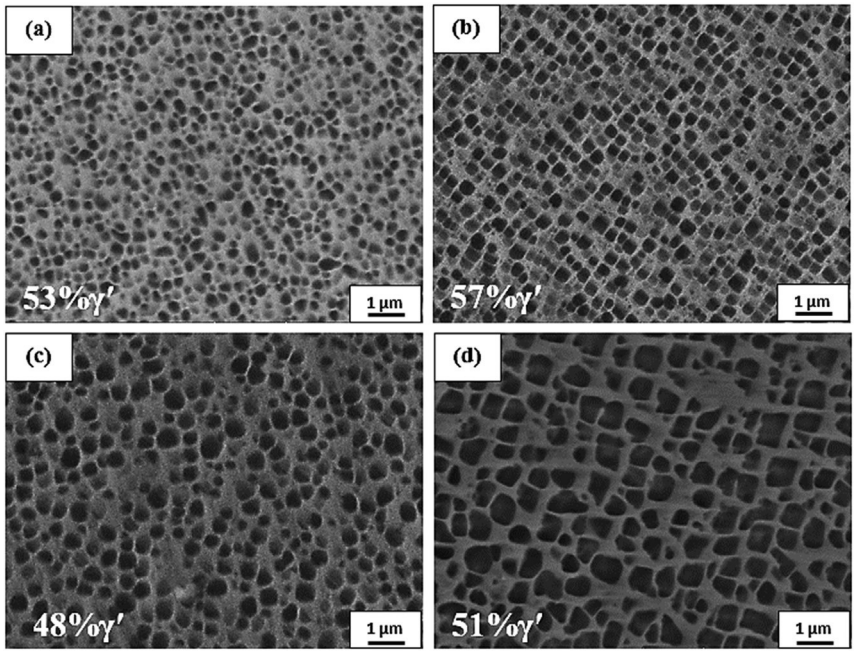

Fig. 9. SEM images of γ′ phases at different heat treating condition: a) CM247-0.1 Zr – 1220 °C/6 h + age, b) CM247-0.1 Zr – 1220 °C/2 h + 1230 °C/4 h + age, c) CM247-0.4 Zr – 1220 °C/6 h + age, d) CM247-0.4 Zr – 1220 °C/2 h + 1230 °C/4 h + age.

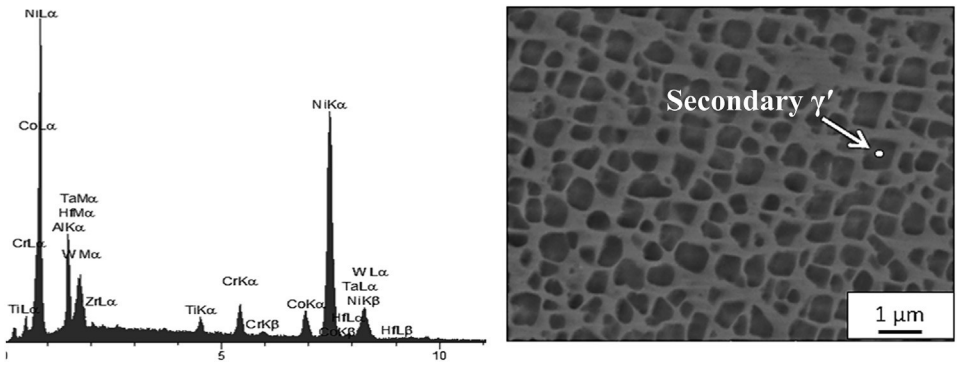

Fig. 10. EDS analysis for γ′ phase in CM247-0.4 Zr alloy at 1220 °C/2 h + 1230 °C/4 h + age condition.

Table 6
Quantitative EDS analysis results for γ′ phase showed in Fig. 10.

Element	Co	W	Cr	Ta	Al	Ti	Hf	Mo	Zr
Wt%	5.78	5.17	3.81	7.77	8.66	1.77	5.38	1.50	1.95
At%	5.93	1.17	4.43	2.60	19.4	2.24	1.82	0.95	1.29

decomposition of primary γ′ precipitates going into solid solution during solution treatment. Thus during the two-step aging the secondary γ′ precipitates grow faster and hence would be coarser.

4. Conclusions

In the present study influence of Zr content on the microstructure and elevated temperature properties of CM247 LC superalloy have been investigated. The results showed that.

1 The volume fraction of γ/γ′ eutectic in CM247-0.1 Zr is about 6%, while in CM247-0.4 Zr it is 14% in the as-cast conditions.
2 The incipient melting temperature for CM247-0.1 Zr is above 1250 °C, while in CM247-0.4 Zr it is below 1220 °C, indicating a systematic growth in incipient melted area as a function of solution treating temperature.
3 An increase in Zr content accelerates the decomposition of primary γ′ precipitates, thus causing the secondary γ′ precipitates grow faster and become coarser after a two-step aging heat treatment. As a result in CM247-0.1 Zr the size of secondary γ′ precipitates falls in 200–400 nm range, while in CM247-0.4 Zr it is in 500–900 nm range after two-step aging.
4 In CM247-0.1 Zr alloy, increasing solution treatment temperature has increased the γ′ volume fraction from 53 to 57% and as a result, has raised the rupture life from 28 to 38 h. However in CM247-0.4 Zr alloy despite the γ′ volume fraction increase from 48 to 51% with solution treatment temperature elevation, the rupture life decrease from 20 to 11.5 h, caused by large incipient melting zones in CM247-0.4 Zr microstructure induced by NiZr phase.

References

[1] K. Harris, G.L. Erickson, Low Carbon Directional Solidification Alloy, U.S. Patent, 5069873, 1991.
[2] K. Harris, G.L. Erickson, R.E. Schwer, MAR M 247 derivations-CM 247 LC DS alloy CMSX single crystal alloys properties & performance, in: R.H. Bricknell, W.B. Kent, M. Gell, C.S. Kortovich, J.F. Radavich (Eds.), Superalloys, TMS, Warrendale, PA, 1984, pp. 221–230.
[3] W.S. Walston, K.S. O'Hara, E.W. Ross, T.M. Pollock, W.H. Murphy, Rene' N6: third generation single crystal superalloy, in: R.D. Kissinger, D.J. Daye, D.L. Anton, A.D. Cetel, M.V. Nathal, T.M. Pollock, D.A. Woodford (Eds.), Superalloys, TMS, Warrendale, PA, 1996, pp. 27–34.
[4] J. Zhang, R.F. Singer, Effect of grain-boundary characteristics on castability of nickel-base superalloys, Metall. Mater. Trans. A 35 (2004) 939–946.
[5] J.B. Wahl, K. Harris, Advanced Ni base superalloys for small gas turbines, Can. Metall. Quart. 5 (2011) 207–214.
[6] J. Zhang, R.F. Singer, Hot tearing of nickel-based superalloys during directional solidification, Acta Mater 50 (2002) 1869–1879.
[7] J. Zhang, Hot tearing in directionally solidified Ni-based superalloys, in: K.A. Green, T.M. Pollock, H. Harada, T.E. Howson, R.C. Reed, J.J. Schirra, S. Walston (Eds.), Superalloys, TMS, Warrendale, PA, 2004, pp. 727–733.
[8] N.R. Muktinutalapati, Materials for Gas Turbines – an Overview, VIT University, India, 2006.
[9] R.C. Reed, The Superalloys Fundamentals and Applications, Cambridge University Press, New York, 2006.
[10] M.J. Donachie, S.J. Donachie, Superalloys a Technical Guide, second ed., ASM International, Ohio, 2002.
[11] J.N. DuPont, J.C. Lippold, S.D. Kiser, Welding Metallurgy and Weldability of Nickel-base Alloys, John Wiley & Sons, New Jersey, 2009.
[12] H.E. Huang, C.H. Koo, Effect of zirconium on microstructure and mechanical properties of cast fine-grain CM 247 LC superalloy, Mater. Trans. 45 (2004) 554–561.
[13] Y. Murata, N. Yukawa, Solid-state reaction for ZrC formation in a Zr-doped nickel-based superalloy, Scr. Metall. Mater. 20 (1986) 693–696.
[14] J.F. Radavich, Effect of Zr variation on the microstructural stability of alloy713C, in: M. Gell (Ed.), Superalloys, TMS, Warrendale, PA, 1968, pp. 199–226.
[15] Y. Murata, N. Yukawa, Solid-state reaction for ZrC formation IN a Zr-doped nickle-based superalloy, Scr. Metall. Mater. 20 (1986) 693–696.
[16] E. Gozlan, M. Bamberger, S.F. Dirnfeld, B. Prinz, Role of zirconium in the phase formation at the interdendritic zone in nickel-based superalloys, J. Mater. Sci. 27 (1992) 3869–3875.
[17] Y. Li, Y. Tang, J. Zhang, Y. Zhu, Z. Hu, Influence of Zr on the solidification behavior and stress rupture property of DZ38 superalloy, Mater. Sci. Prog. 7 (1993) 1–7.
[18] J. Zhang, R.F. Singer, Effect of Zr and B on castability of Ni-based superalloy IN792, Metall. Mater. Trans. A 35 (2004) 1337–1342.
[19] P. Zhou, J. Yu, X. Sun, H. Guan, Z. Hu, Roles of Zr and Y in cast microstructure of M951 nickel-based superalloy, Trans. Nonferr. Metal. Soc. 22 (2012) 1594–1598.
[20] S. Xie, T. Wang, J. Lu, H. Yang, Effects of Zr on microstructure and short-term strength in GH586, J. Mater. Sci. Technol. 15 (1999) 415–418.
[21] J.M. Nell, N.J. Grant, Multiphase strengthened nickel base superalloys containing refractory carbide dispersions, in: S.D. Antolovich, R.W. Stusrud, R.A. MacKay, D.L. Anton, T. Khan, R.D. Kissinger, D.L. Klarstorm (Eds.), Superalloys, TMS, Warrendale, PA, 1992, pp. 113–121.
[22] R.K. Sidhu, O.A. Ojo, M.C. Chaturvedi, Sub-solidus melting of directionally solidified Rene 80 superalloy during solution heat treatment, J. Mater. Sci. 43 (2008) 3612–3617.